# An Ab Initio Molecular Dynamics Study on the Hydrolysis of the Po(IV) Aquaion in Water

**Regla Ayala,[†] Riccardo Spezia,[‡] Rodolphe Vuilleumier,[§] José Manuel Martínez,[||] Rafael R. Pappalardo,[||] and Enrique Sánchez Marcos*,[||]**

*Departamento Química Inorgánica, Universidad Sevilla, CSIC, ICMSE, Seville 41012, Spain, Laboratoire Analyse et Modélisation pour la Biologie et l'Environnement, Université d'Evry Val d'Essonne, UMR 8587 CNRS, Bat Maupertuis, Bd F. Mitterrand 91025 Evry, Cedex, France, Département de Chimie de l'École Normale Supérieure, 24 rue Lhomond, 75005 Paris, and Departamento Química Física, Universidad Sevilla, E-41012 Seville, Spain*

*Received: February 4, 2010; Revised Manuscript Received: July 7, 2010*

Po(IV) in water has been studied by means of Car−Parrinello molecular dynamics (CPMD) simulations. A new Trouiller−Martins pseudopotential for Po(IV) has been developed. This pseudopotential was tested by comparing the structure and energetics of small $[Po(H_2O)_n(OH)_m]^{4-m}$ clusters optimized quantum-mechanically. CP-MD simulations of 1 Po + 60 $H_2O$ were carried out starting from three different degrees of hydrolysis of the aquaion ($m = 0$, 2, and 3), in order to check the stability of the hydrolyzed forms under the simulation conditions. The three simulations converge to a description of the solution where the same hydrolyzed species are present. Dynamics of the octahydrate aquaion in water indicates that dehydration couples to hydrolysis processes, and the total coordination number decreases with the hydrolysis degree. The time evolution of the initial $[Po(H_2O)_8]^{4+}$ aquaion in aqueous solution indicates that hydrolysis precedes to dehydration in the process from aquaion to hydroxoaquaion. Structural and dynamical properties of the ligands in the first coordination shell are analyzed. The power spectra and its contribution from fragments of the first coordination shell are also examined.

## 1. Introduction

It is well known that multivalent cations in aqueous solutions can participate in a series of consecutive hydrolysis reactions.[1,2] In the case of tetravalent cations, hydrolysis processes as well as polynucleation, colloid formation, and redox processes may occur as a function of different medium conditions, such as pH, concentration, additives, etc.[1−4] The vast chemistry of actinides and its technological applications have led to the experimental study of a series of tetravalent cations in aqueous solutions, such as Th(IV), U(IV), Np(IV), and Pu(IV). The investigation of their hydrolysis processes and the determination of the corresponding equilibrium constants have shown the complexity of their solution chemistry.[4−8] This seems to be the case for the solution chemistry of the radioactive cation Po(IV), although very few experimental information has been reported.[9,10] The research on polonium ion aqueous solutions is mainly hindered by two serious obstacles. First, it is rare in nature. In fact, the abundance of Po in natural minerals is at the trace level, and its extraction involves extremely complex operations. Nowadays, the main source of Po is artificial coming from nuclear reactions. Although there is not a quantitative estimation of Po production, it seems to be of the order of some hundreds of grams per year. Second, the high toxicity of this element has prevented the study of its physicochemical properties in different media and conditions. Therefore, this is a particularly suitable case where computational chemistry can help in filling the gap represented by experimental limitations and may provide an atomistic insight into the structure and dynamics of polonium ion in solution. There is only a few number of computer simulations of tetravalent aqua ions in water. One of them is devoted to the Th(IV) by Yang et al.[11,12] using intermolecular potentials based on the hydrated ion approach developed by our group.[13] Due to the classical nature of this molecular dynamics (MD) simulation, hydrolysis processes were not taken into account. Rode and co-workers have recently applied their quantum mechanics/molecular dynamics (QM/MD) model to the case of U(IV),[14] but they only examine the hydration structure of the aquaion.

In our previous QM studies of Po(IV) in aqueous solutions applying semicontinuum solvation models,[15,16] we have verified its strong tendency toward hydrolysis. The phenomenon has a significant impact on the coordination number, ranging from 8−9 in the aquaion case to 4 for the $[Po(OH)_4]$ hydroxide. In this sense, the polonium hydrolysis can be envisaged as a chain of proton elimination and dehydration reactions transforming aquaions into hydrolyzed species. However, on the basis of these results, it is not possible to know the mechanism of the proton elimination and dehydration reactions. One can wonder if it was first the deprotonation or the dehydration processes or if both processes take place simultaneously. It was also found that the Po(IV)−ligand (ligand being $H_2O$ or $OH^-$) potential energy surfaces (PES) are rather flat, and more than one species can coexist simultaneously under the same medium conditions. These results were obtained considering explicitly the ion and its first solvation shell, whereas outer solvent molecules were represented by a dielectric continuum. Although it has been proven[17−19] that these semicontinuum methods can provide reliable results, the absence of some specific interactions beyond the first hydration shell along with the flatness of the PES of the system compels us to carry out ab initio molecular dynamics simulations where statistical averages are accounted for to

* To whom correspondence should be addressed. E-mail: sanchez@us.es.
[†] Departamento Química Inorgánica, Universidad Sevilla.
[‡] Université d'Evry Val d'Essonne.
[§] École Normale Supérieure.
[||] Departamento Química Física, Universidad Sevilla.

10.1021/jp1010956 
Published on Web 08/09/2010

properly describe Po(IV) hydration. In addition, a variety of Po(IV)−solvent species and their associated processes may be observed as time proceeds as well as the estimation of dynamics properties of the system, not available from the previous static QM studies. What's more, the description of all the species at the same level of calculation allow us to evaluate the competition between polonium ion−ligand and ligand−solvent interactions, which plays a significant role in the extension of the hydrolysis processes. The possibility of studying the nature and equilibria of these hydrated/hydrolyzed structures is of fundamental interest because the diffusive and migrative behavior of the ion as well as its reactivity can strongly depend on them.

This paper studies the dehydration and hydrolysis processes of Po(IV) using Car−Parrinello molecular dynamics (CPMD) simulations. Thus, the previous results obtained by semicontinuum models,[15,16] are now extended to a dynamical view of the local environment and mechanistic description of the aquaion evolution among the possible hydrolyzed species. This study allows us to gain insight into the understanding of the specific interactions playing a significant role in these complex equilibria. Previous ab initio MD studies on the hydrolysis of trivalent cations, such as Cr(III) or Fe(III) have already supplied a reasonable microscopical description of the deprotonation process.[20,21] Additionally, this work explores the potentiality of the ab initio MD methods to provide a first-principles description of the dynamic protonation/deprotonation equilibrium between different hydrolyzed forms of the Po(IV) aquaion.

## 2. Methodology

**2.1. Electronic Structure.** Plane-wave implementation of density functional theory (DFT) was used to describe the electronic structure with the BLYP functional,[22,23] a generalized gradient approximation (GGA) to the exchange-correlation functional. Only valence electrons were considered in the electronic structure, the core electrons were approximated through the use of pseudopotentials.

A new Po pseudopotential (PP) for the BLYP functional has been developed. A Goedecker−Tetter−Hutter type Po PP is available for the local density approximation (LDA) functional.[24−26] However, this functional is not accurate enough for simulating liquid water, as it overestimates water−water interactions and leads to poor results for both structure and energetics.[27] We have developed a norm-conserving Trouiller−Martins (TM)-type PP,[28] which, when used with TM oxygen and hydrogen PPs, was shown to provide accurate description of ion hydration.[29] Po(II) was chosen as a reference state, in the configuration $[Xe]4f^{14}5d^{10}6s^26p^2$. Scalar relativistic corrections were used for the reference calculation, and potentials were then generated for the 6*s*, 6*p*, and 6*d* channels with cutoff radii (in Bohr) $R(6s) = 1.72$, $R(6p) = 2.10$, and $R(6d) = 3.30$. Furthermore, a nonlinear core correction (NLCC)[30] was applied with a cutoff radius $r_0 = 1.81$ Bohr. The Kleyman−Bylander scheme[31] for the separation of angular momenta was applied, setting the $l = p$ term as the local term. For oxygen and hydrogen, we have used standard TM pseudopotentials, as in several Car−Parrinello studies,[32] employing the semilocal Kleinman−Bylander decomposition.[31] With these PPs, the Kohn−Sham orbitals were expanded in planewaves (PWs) up to a kinetic energy cutoff of 110 Ry.

This setup, and in particular the reliability of the new Po PP, was tested by comparing structure and energetics of small $[Po(H_2O)_n(OH)_m]^{4-m}$ clusters, with $1 \le n \le 9$ and $0 \le m \le 3$, with respect to a reference calculation. These clusters were optimized at the MPW1MPW91 level using DZ basis sets (see ref 16 for details) and with the PW method. In the PW calculations of these clusters, no periodic boundary conditions were applied but a screening method[33] was used. A good agreement of the planewave-pseudopotential (PW/PP) method with the reference calculation in both structure and energetics was found, then this setup was further used for the ab initio simulations of polonium aqueous solutions.

**2.2. Ab Initio Simulations of Aqueous Solutions.** Ab initio molecular dynamics simulations using the Car−Parrinello scheme[34] on a system containing 1 Po(IV), 60 oxygen atoms, and 120 hydrogen atoms in a box with an edge size of 12.898 Å were performed. Periodic boundary conditions were applied at the Γ point approximation; an homogeneous charge background compensates for the positive charge of the system. All simulations were run in the NVT ensemble, and the temperature was kept around $T = 300$ K using a Nosé-Hoover chain of thermostats on the ionic degrees of freedom.[35−37] The time-step employed was equal to 4 au (0.12 fs) and the fictitious mass of the additional electronic degrees of freedom was 450 au. All plane-wave calculations were performed using the CPMD code.[38]

Three different trajectories were run. The first one, hereafter labeled A), was begun from an octahydrate of Po(IV) ($[Po(H_2O)_8]^{4+}$) plus 52 water molecules. The second trajectory, hereafter labeled B), started from a system containing a $[Po(H_2O)_3(OH)_3]^+$ cluster plus 51 water molecules and 3 $H_3O^+$ species. The third trajectory, hereafter labeled C), was initiated from a system containing a $[Po(H_2O)_4(OH)_2]^{2+}$ cluster plus 52 water molecules and 2 $H_3O^+$ species. In simulations B and C, the $H_3O^+$ species were located at the edge of the simulation box as previous CPMD tests carried out in our group using the LDA functional indicated. It is worth pointing out that the three simulations have the same atomic composition although the initial distribution of $H_2O$, $H_3O^+$, and $OH^-$ species is different. The $[Po(H_2O)_4(OH)_2]^{2+}$ and $[Po(H_2O)_3(OH)_3]^+$ stoichiometries of simulations C and B, respectively, were chosen as an initial configuration on the basis of our previous semicontinuum results where these aggregates were revealed as the most stable species in aqueous solutions.[16] The evolution of these simulations was analyzed studying (i) the similarities or differences in the final degree of hydrolysis obtained as a function of the initial configuration, (ii) the stability of the different Po(IV) species in solution as well as their possible interconversion among them, and (iii) the relaxation dynamics of the Po clusters. The systems were equilibrated for around 3−7 ps followed by at least 26 ps of data collection. Configurations were saved every 10 steps for further analysis.

It is worth establishing at this point the microscopical framework of this study and its relationship with macroscopical behavior and the particularly complex dependency of their thermodynamic properties of medium factors, such as pH, counterions, ionic strength, etc.[2,3,6] The chemical behavior of a highly charged metal ion in aqueous solution enhances the acidity of coordinated water molecules promoting their deprotonation.[39] The extent of the deprotonation is controlled by quantum-mechanical (QM) factors associated with the cation and the closest water environment, as well as by macroscopic factors appearing from the bulk of the solution. The present ab initio MD study is restricted to the first factors. Some interesting methods based on the idea of coupling a pH-bath to the simulated system have recently been proposed in the literature in the context of classical MD simulations of biomolecules.[40,41] Extension to ab initio MD simulations is not affordable at the current state of the art due to both the size of systems and the

**TABLE 1: Formation Energies in kcal/mol for the $[Po(H_2O)_n(OH)_m]^{4-m}$ Clusters with *n* and *m* between 1 and 9, and 0 and 3, Respectively, Using MPW 1PW91 and DZ Basis Sets and BLYP and TM Pseudopotentials Together with PWs (PP/PW)**

| | $\Delta E$ (kcal/mol) | |
|---|---|---|
| *n*,*m* | MPW1PW91 | PP/PW |
| 1,0 | −249.7 | −266.5 |
| 2,0 | −434.9 | −456.1 |
| 3,0 | −572.4 | −589.4 |
| 4,0 | −669.6 | −686.4 |
| 6,0 | −825.8 | −838.5 |
| 8,0 | −929.4 | −923.8 |
| 9,0 | −951.0 | −950.6 |
| 0,1 | −918.4 | −931.1 |
| 5,1 | −1305.6 | −1304.9 |
| 4,2 | −1682.2 | −1672.6 |
| 3,3 | −1955.1 | −1936.5 |

simulation time. However, the use of three simulations of the same system with different starting ratios between the hydrolysis degree of the Po(IV) aquaion and the number of $H_3O^+$ ions allow us to circumvent in some way this limitation. Given that the conditions of the system are defined, and, in an efficient way, a range of protonation/deprotonation equilibrium, without including any bias in the simulations, is explored. Then, we are able to provide a first-principles description of the deprotonation/protonation process coupled to the dynamics of the local environment.

## 3. Results and Discussion

**3.1. Gas Phase Clusters: Structure and Energetics.** The formation energies of the clusters mentioned in the Methodology section are collected in Table 1 and the optimized structures are displayed in Figure 1.

The arrangements of ligands around the polonium ion in the PP/PW structures are very close to those of MPW1PW91 and DZ basis sets (see Figure 1). As a rule, Po−O distances are slightly longer in the case of PP/PW results (in blue in Figure 1). As expected for a more ionic character of the Po−O(OH) bond than that of the Po−O($H_2O$) bond, the Po−O(OH) bond lengths are shorter than the Po−O($H_2O$) ones by 0.3−0.7 Å, as a function of the number of hydroxyl ligands in the Po complexes.

In our previous QM study on Po(IV) aquaions,[15] their structures were rationalized on the basis of the nature of the bonding. This way, the water molecules were not symmetrically distributed around the ion, but their arrangement reveals O−Po−O angles around 90 or 180°. This is due to the bonding nature of Po−$H_2O$, which is mainly dominated by the 6*p* orbital of the polonium ion with no contribution of its 6*s* orbital. These types of structures were well-reproduced by what we have labeled as PP/PW results (see structures b−e in Figure 1). Likewise, in the previous QM studies about Po(IV) hydrolysis,[16] aquaions and hydrolyzed species showed that structures with the same number of ligands adopt similar arrangements, although some differences can be identified. The most significant difference was that water molecules in trans positions with respect to $OH^-$ ligands exhibit longer distances from polonium than the rest of water molecules. This behavior is also well-reproduced by the new PP. For example, the $[Po(H_2O)_5)(OH)]^{3+}$ cluster, which presents a distorted octahedral structure, has the water molecule opposite to the hydroxyl ligand ($H_2O$ in the lower side of cluster j in Figure 1) at a longer distance to the Po ion than the rest of water molecules of the cluster. The same trend can be observed for the $[Po(H_2O)_4(OH)_2]^{2+}$ and $[Po(H_2O)_3(OH)_3]^+$ clusters (k and l in Figure 1). Another peculiarity of the partially hydrolyzed aquaions is that when two or more $OH^-$ ligands are present, the adopted arrangements are such that hydroxyl groups are not opposite to each others. The same structural pattern was obtained in the optimization processes of Po clusters using the new Po PP. Therefore, the new PP describes well the differences between the two types of ligands.

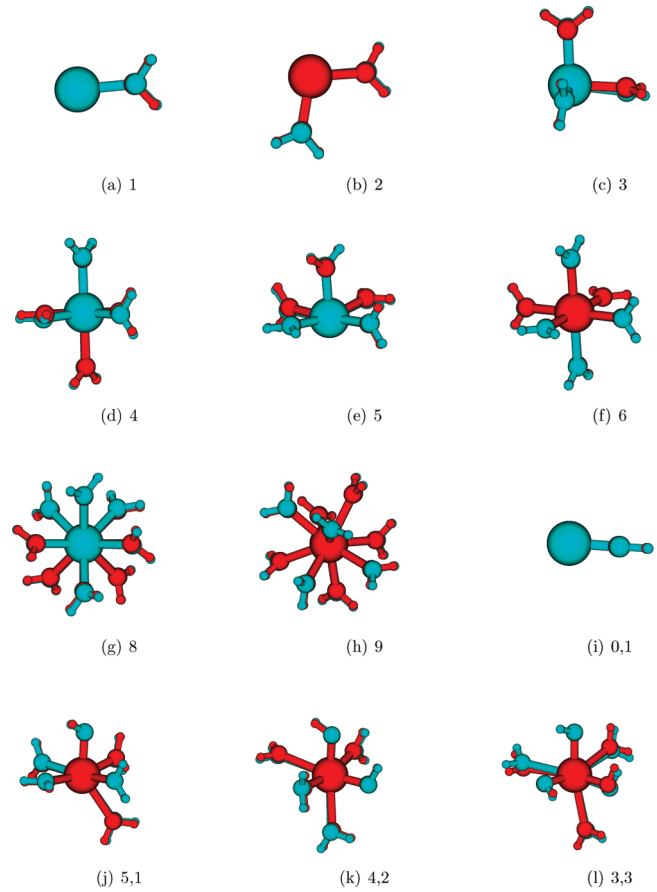


**Figure 1.** Comparison of optimized structures obtained by MPW1PW91 and DZ basis sets from refs 15 and 16 and BLYP and TM pseudopotentials together with PWs (PP/PW). The structures have been overlapped. The atoms in red correspond to MPW1PW91 and DZ basis sets results, whereas atoms in blue are PP/PW results. The labels (*n*,*m*) indicates the number of water molecules and hydroxyl groups, respectively, in the cluster.

Formation energies were computed as

$$\Delta E = E_{[Po(H_2O)_n(OH)_m]^{(4-m)+}} - E_{Po^{4+}} - nE_{H_2O} - mE_{OH^-}$$

Table 1 shows that the differences in the estimation of formation energies using PP/PW are lower than 7% for aquaions and 2% for hydrolyzed species compared to MPW1PW91 and DZ basis sets results. Interestingly, these differences decrease as the size of the cluster increases. Despite these discrepancies, the relative order of stability among the clusters is maintained, having more favorable formation energies than those clusters that present a higher degree of hydrolysis.

The convergence of all these features indicates that the similarities between the two sets of results (DZ basis sets MPW1PW91 and PP/PW) regarding both the structural and energetic data allows us to be confident on the reliability of the

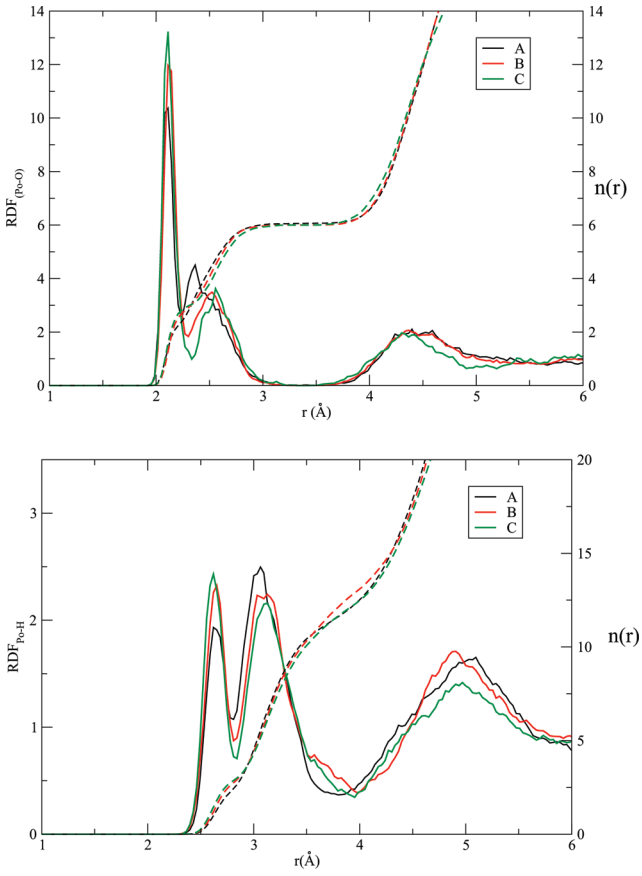


**Figure 2.** (a) Po−O RDFs (solid lines) and running integration numbers, ($n(r)$), (dashed lines) for simulations A, B, and C. (b) Po−H RDFs (solid lines) and running integration numbers, ($n(r)$), (dashed lines) for simulations A, B, and C.

Po PP along with the CPMD results of condensed matter where it is employed.

**3.2. Condensed Matter.** ***3.2.1. Structure.*** The Po−O radial distribution functions (RDFs) and their integration numbers ($n(r)$) for the three CPMD simulations detailed in the Methodology section are depicted in Figure 2a. A well-defined first solvation shell is observed in the three cases, $n(r)$ integrating to six oxygen atoms at 3.3 Å. The first solvation shell is defined by the two first peaks in the Po−O RDFs. The first peak in the three RDFs is centered at the same position (∼2.1 Å). However, the height is different depending on the simulation. The running integration numbers span from 2.5 to 3.0 oxygen atoms. The second peak, which still corresponds to the first coordination shell, is quite dependent on the simulation. The maximum of this peak is centered at 2.4, 2.5, and 2.6 Å for simulations A, B, and C, respectively. Bearing in mind that simulation A begun from an octa-coordinated aquaion, a decrease in the total coordination number, which will be discussed below, took place during the simulation time. In contrast, simulations B and C have maintained the initial number of oxygen atoms in the local arrangement of the Po(IV). The uncompleted convergence in the structure of the first solvation shell for the three Po−O RDFs might indicate that the average structural situation described by these simulations is rather dependent on the different initial configurations. As it will be shown later, the average situation is an equilibrium between the same species but with a different ratio among simulations. This fact is due to the limited amount of CPMD simulation time that is possible to average with nowadays available computing resources, providing not identical Po−O RDFs. Beyond the second peak of the first coordination shell, the Po−O RDFs goes down to zero, which indicates that there is no significant exchange of oxygen atoms between the first and further solvations shells, at least in the time scale of our simulations (∼26 ps.). The third peak of Po−O RDFs, corresponding to the second solvation shell, is wide and centered at 4.4−4.5 Å, integrating up to 10−12 O atoms.

The analysis of the Po−H RDFs shown in Figure 2b indicates that they are more similar among them than the Po−O RDFs: maxima and minima are roughly at the same positions. The first and second maxima, corresponding to the first solvation shell, are at ∼2.6 and 3.1 Å, respectively. A third peak in the Po−H RDFs is well-described at ∼5 Å. It is interesting to point out that, unlike Po−O RDFs, the Po−H RDFs do not present a depletion zone between the first and second hydration shells, that is, H atoms move from the first to the outer solvation shells and vice versa during the simulation time. The running integration number of the first peak is 2.4, 2.7, and 2.9 for simulations A, B, and C, respectively. The second peak integrates roughly to 8.6, 10.1, and 9.3 H atoms for simulations A, B, and C, respectively. A clear assignment of the Po−H RDF peaks with solvation shells is not as simple as in the case of the Po−O RDFs and a fraction of the H atoms of the second hydration shell are included in the second peak of the Po−H RDFs. This explains that the running integration number of this peak is larger than the corresponding for six ligands in the first hydration shell, (i.e., 9 hydrogen atoms for $[Po(H_2O)_3(OH)_3]^+$ or 10 hydrogen atoms for $[Po(H_2O)_4(OH)_2]^{2+}$).

When Po−O and Po−H RDFs are examined together, the first peak in both cases integrates to the same number of atoms (2.5−3.0). This means that the first peak corresponds to the O and H atoms of the hydroxyl groups. The number of H atoms in the second peak is roughly twice that corresponding to O atoms, so that the second peak can be mainly assigned to water molecules. According to the Po−O and Po−H RDFs, there is a total number of six ligands in a distorted octahedral local arrangement of the Po ion that is defined by 2−3 hydroxyl groups and 4−3 water molecules. On the basis of these results, an equilibrium between $[Po(H_2O)_4(OH)_2]^{+2}$ and $[Po(H_2O)_3(OH)_3]^+$ species in the three simulations may be envisaged. Nonetheless, the ratio of the species involved in the equilibrium is not exactly the same due to the lack of statistics. Although in the context of ab initio molecular dynamics (AIMD) simulations, the length of the three simulations is not negligible, it seems insufficient for a convergence of the structural results when quite different initial Po-hydroxoaquaion configurations have been selected. However, for a complete convergence of the three simulations, it would have needed trajectories of longer time scale that are not affordable with current computing resources.

The equilibrium between Po(IV) species previously proposed, ($[Po(H_2O)_4(OH)_2]^{+2}$ and $[Po(H_2O)_3(OH)_3]^+$), is illustrated in Figure 3, where the time evolution of the Po−O distances of the oxygen atoms directly bonded to the Po ion is plotted. There are two well-separated distances as shown in the RDFs, one distance at ∼2.1 Å corresponding to hydroxyl groups, and the other at 2.4−2.9 Å corresponding to water molecules. It is worth pointing out that this wide gap in the Po−O($H_2O$) distance comes from the general structural effect induced by the $OH^-$ ligands coordinated to the metal ion, which labilizes water molecules located in the first coordination shell.[42] In particular, the structural trans effect is responsible of the lengthening of the Po−O distance of the water molecule opposite to the hydroxide group.[16] Figure 3 shows how Po−O distances are mainly fluctuating around either 2.1 or 2.6 Å for the three

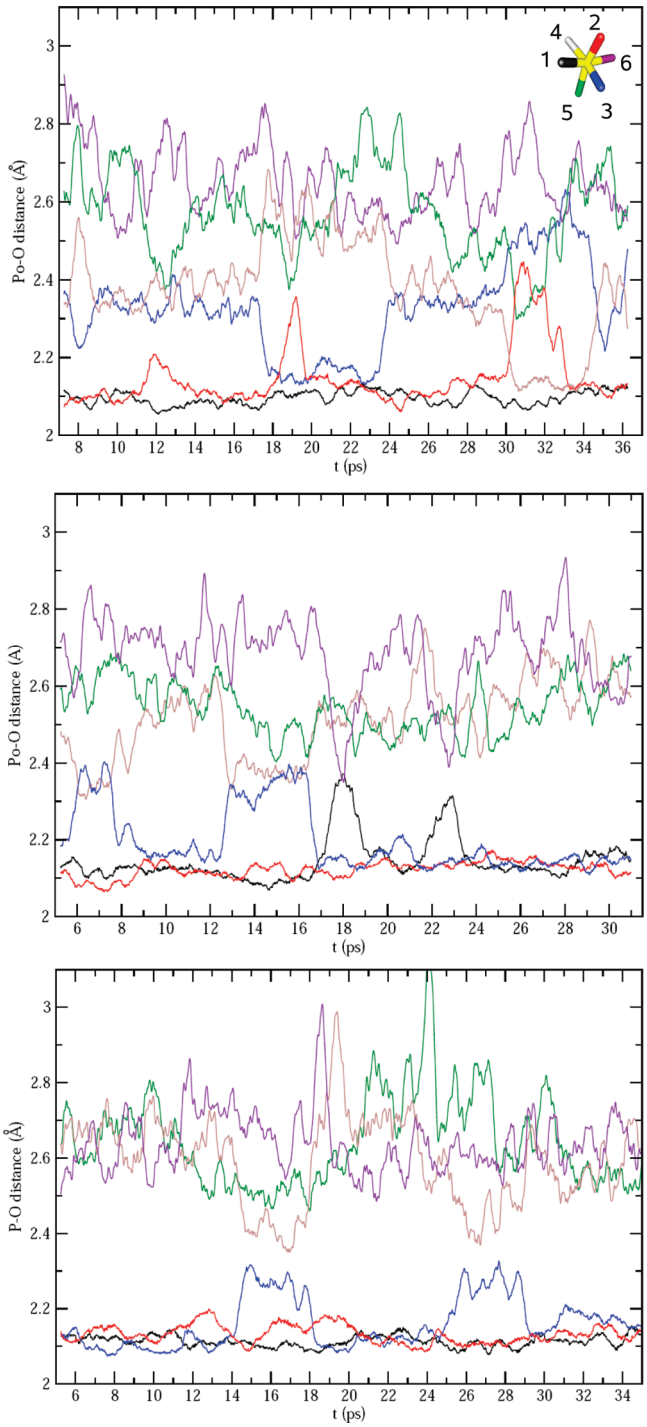


**Figure 3.** Evolution of Po−O first shell distances (in Å) along the simulation time from simulations A (top), B (center), and C (bottom).

simulations. However, there are some intervals in the trajectory where the Po−O distance of some ligands (see for example distances labeled as 3 (blue line) for simulations A, B, and C) changes their average values from 2.1 to 2.3 Å and from 2.3−2.6 to 2.1 Å, indicating that these atoms are involved in protonation/deprotonation processes along the simulation time. The same tendency appears in the simulations coupling the change in the Po−O distances affected by the trans effect. This is nicely illustrated when the Po−O distances of the O atom involved in hydrolysis processes and the O atom opposite to the former are analyzed. (See, for example, simulation C, in the range around 14−18 and 25−29 ps; the Po−O distance of the ligand labeled as 3 (blue line) in Figure 3 increases from 2.1 up to 2.3 Å.) In parallel, the Po−O distance of the water molecule labeled as 4 (gray line) in the graphics decreases from 2.6 to 2.4 Å. This is because when a protonation of the hydroxyl group takes place, the trans effect exerted by this group on the water molecule opposite to it disappears and consequently the Po−O distance related with this water molecule decreases. Then, both Po−O distances tend to collapse on a similar value close to that of a Po−O($H_2O$) bond. After 4 ps the oxygen atom, labeled as 3 (blue line) in Figure 3, forming part of a water molecule goes through a hydrolysis process that decreases the Po−O distance to the initial values (close to 2.1 Å). The water molecule opposite to this O atom, labeled as 4 (gray line) in Figure 3, increases its Po−O distance due to the trans effect mentioned previously. Although only explained in detail for simulation C, this correlation in the Po−O distances of the O atoms involved in hydrolysis processes and the water molecules opposite to them is present in all simulations (for example, oxygen atoms 3 (blue line) and 4 (gray line) in the interval 18−24 ps in simulation A or oxygen atoms 3 (blue line) and 4 (gray line) in the interval 13−16 ps in simulation B).

In our previous QM study,[16] we also found that when two or more $OH^-$ groups become part of the first solvation shell of the polonium ion, they avoid being opposite to each other, that is, in a trans arrangement. We only observed $OH^-$ opposite to each other in the case of clusters containing four $OH^-$ groups. The same conclusion is hold up when a dynamics simulation of the hydroxo aquo complexes is carried out. When the trajectories of simulations A, B, and C are analyzed, no species with four $OH^-$ groups are formed under our AIMD simulation conditions and, for the rest of less hydrolyzed species, no $OH^-$ groups opposite to each other were observed in any of the computed trajectories. The fact that $[Po(H_2O)_n(OH)_4]$ clusters are not representative in Po(IV) aqueous solutions is also consistent with our previous[16] studies of Po(IV) hydration using QM semicontinuum models where the free energy associated with the $[Po(H_2O)_n(OH)_4]$ cluster formation was either negligible or positive.

***3.2.2. Protonation, Deprotonation and Dehydration Processes.*** The relaxation processes related to the rearrangements of the Po(IV) environment that took place from the initial configuration up to reach the dynamical equilibrium are different depending on the simulation, as expected when their starting points are different and their final distributions are similar. During the equilibration period, different processes were identified and have been summarized in the plot shown in Figure 4. Thus, for the case of simulation A, the initial configuration around the polonium ion was an octahydrate. After 0.3 ps, the first hydrolysis process took place, and the octahydrate became a hydrolyzed species with seven water molecules and one hydroxyl group in the first hydration shell. For 6 ps, the dynamics of the monohydroxo Po aquaion was observed. At 6.2 ps, a second hydrolysis process took place, and the local arrangement of the Po ion ended up in six water molecules and two hydroxyl groups. From this moment a gradual decrease in the solvation number was observed going from six down to four water molecules in the first solvation shell, whereas the number of hydroxyl groups remained constant. The decrease in the coordination number can be noticed by plotting the partial Po−O RDFs at different time intervals in simulation A (Figure 5). The first interval corresponding to 0−0.3 ps (black line) presents a noisy Po−O RDF with a unique peak in the first hydration shell and an integration number equal to 8. In the second interval, from 4 to 7 ps (red line), the integration number stays constant,

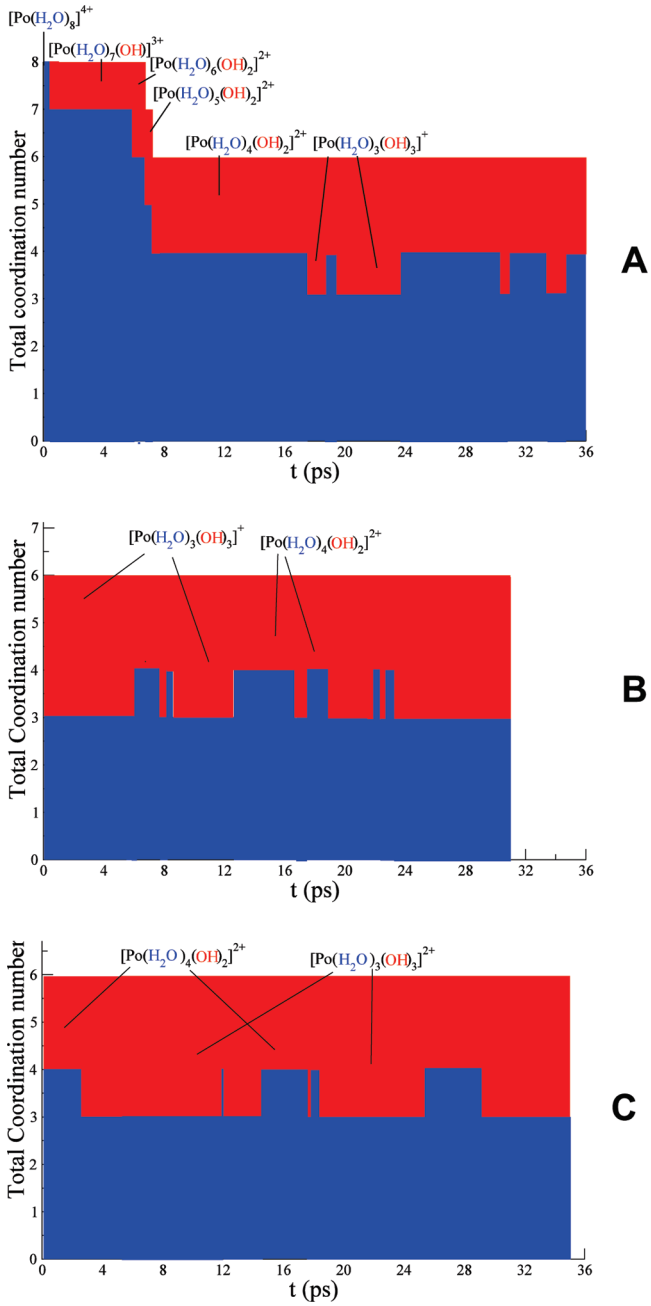


**Figure 4.** Time evolution (bar charts) of the Po environment in terms of dehydration and hydrolysis processes from the initial configuration of the three simulations: (A) $[Po(H_2O)_8]^{4+}$; (B) $[Po(H_2O)_3(OH)_3]^{+}$; (C) $[Po(H_2O)_4(OH)_2]^{2+}$. Total bar height gives the total coordination number. Red and blue portions of the bar are proportional to the number of the hydroxyl group and water molecules in the cluster.

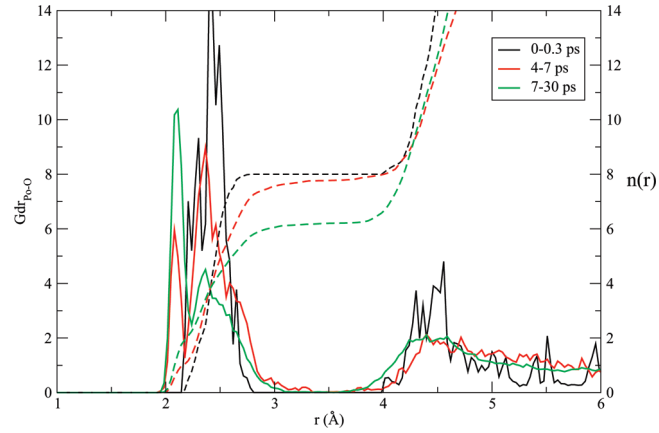


**Figure 5.** Partial Po−O RDFs (solid lines) and running integration numbers, ($n(r)$), (dashed lines) for simulation A in the intervals 0−0.3 ps (black), 4−7 ps (red), and 7−30 ps (green).

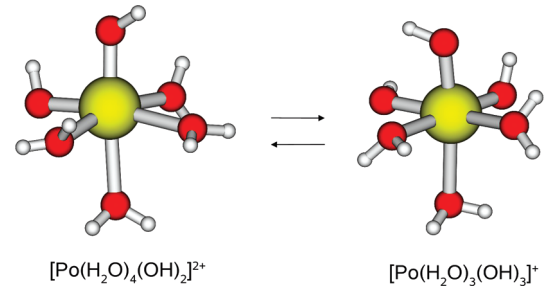


**Figure 6.** Equilibrium and predominant geometries found in simulations A, B, and C under the medium conditions imposed by our methodology.

but a splitting of the first peak appears: the peak at shorter distance corresponds to the hydroxyl group, and the other to the rest of the water molecules. In the third interval, from 7 to 30 ps (green line), the integration number goes down to 6. Bearing in mind the evolution of simulation A, it can be concluded that there is a close relation between the coordination number of the first solvation shell of the Po ion in aqueous solutions and its hydrolysis degree. The more hydrolysis, the fewer the number of ligands in the first solvation shell. This conclusion derived from a dynamical monitorization of the initial Po(IV) aquaion is fully consistent with the previous QM semicontinuum results derived from a static analysis.[16] The dynamic description supplied by the CPMD simulations allows us to gain insight into this idea by adding time evolution: the dehydration process occurs after the hydrolysis process has taken place, during the relaxation period. For simulations B and C, Figure 4 illustrates that the rearrangement observed during the thermalization time was less significant since the number of ligands around the Po ion was already six at the beginning of the simulation, then only protonation and deprotonation processes were observed along all the simulation time, defining an equilibrium between the dihydroxo and trihydroxo Po complexes.

Once the thermalization period is ruled out in all the simulations, their results can be analyzed on the same foot. Along the trajectories, different protonation and deprotonation processes occurred. The oxygen atoms involved in these processes are those that changed their distances to the Po ion between two different sets of values (2.1 and 2.3, or 2.4−2.6 and 2.1 Å) as shown in Figure 3. This way, $[Po(H_2O)_4(OH)_2]^{+2}$ and $[Po(H_2O)_3(OH)_3]^{+}$ complexes can be considered the most stable species under simulation medium conditions leading to an equilibrium mainly dominated by these two species (Figure 6). This may also be seen when the O(first shell)−H RDFs are plotted. Figure 7 displays the O−H RDFs of the O atoms of the first solvation shell for the three simulations. According to Figure 7, three different types of O atoms can be identified: O atoms that belongs to a hydroxyl group (labeled 1 in simulation A, 2 in simulation B, and 1 and 2 in simulation C in Figure 7), O atom corresponding to a water molecule (labeled 5 and 6 in simulation A and 4, 5, and 6 in simulation B and C in Figure 7), and O atom involved in protonation and deprotonation events (labeled 2, 3, and 4 in simulation A, 1 and 3 in simulation B, and 3 in simulation C in Figure 7). The running integration numbers for the first peaks of the two first types of oxygen atoms are 1 and 2, respectively, as expected for a hydroxyl group and

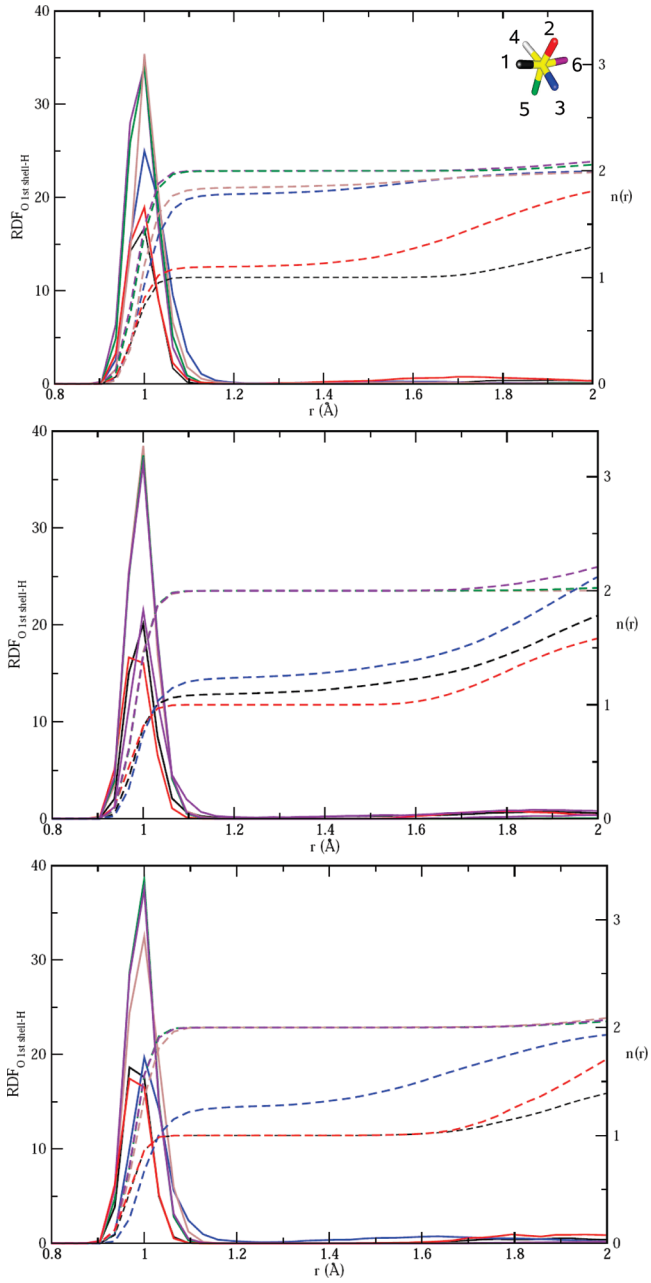


**Figure 7.** O(first shell)−H (solid lines) and running integration numbers, ($n(r)$), (dashed lines) for simulations A (top), B (center), and C (bottom).

a water molecule (see n($r$) value at $r \sim 1.3$ Å). Nonetheless, the running integration number of the O atom involved in the hydrolysis processes is larger than 1 and smaller than 2. The proximity to one of these two extreme values gives an idea about the identity of these O atoms along the trajectory. A value close to 2 would indicate that the O atoms mainly form water molecules, whereas a value close to 1 would give an idea of a hydroxyl group. A value close to 1.5 would show that the oxygen atom is involved in a hydroxyl form and in a water molecule during similar periods along the simulation, and consequently is participating in a series of protonation and deprotonation events. On the basis of Figure 7, it is possible to estimate the ratio of each cluster ($[Po(H_2O)_4(OH)_2]^{+2}$ and $[Po(H_2O)_3(OH)_3]^{+}$) along the simulation. The ratio of the $[Po(H_2O)_4(OH)_2]^{+2}$ species is larger in simulation A because there are four O atoms with an integration number close to 2 and two O atoms with an integration number close to 1. The

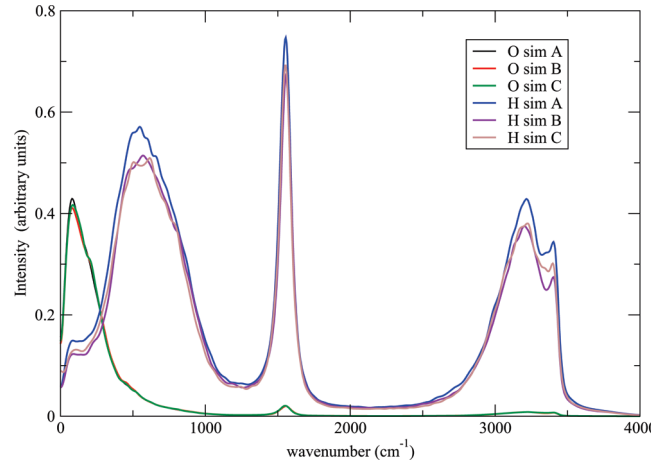


**Figure 8.** Power spectra of the O and H atoms for simulations A, B, and C.

$[Po(H_2O)_3(OH)_3]^{+}$ species is predominant in simulations B and C because there are three O atoms with an integration number close to 2 and three O atoms with an integration number close to 1. This is also consistent with the results plotted in Figure 4.

The analysis of the trajectories indicates, to a certain extent, that there is a common pattern for the loss and gain of the proton responsible for the change between the $[Po(H_2O)_4(OH)_2]^{+2}$ and $[Po(H_2O)_3(OH)_3]^{+}$ species. These lost protons stay close to the oxygen atoms to which they were originally attached and return after a few picoseconds. Thus, the hydrolysis processes connecting the species can be seen as a forward and backward path of the involved proton, or temporary protolysis, as it has already been reported in some previous ab initio MD simulations of other divalent[43] and trivalent[20,21] metal cations.

***3.2.3. Power Spectra.*** The dynamics of the H-bonding plays a central role in many fundamental phenomena occurring in aqueous solutions. It is interesting to analyze the effect of Polonium ion on the H-bond network of its surrounding solvation shells and to check whether this effect could be used to estimate its hydrolysis degree. To fulfill these objectives, we have computed the vibrational spectra associated with the O and H atoms of our systems. These spectra were computed as the temporal Fourier transform (FT) of the velocity autocorrelation (VAC) functions of the O and H atoms. The study of the vibrational density of states (VDOS) spectra from VAC functions comes from the NVT simulations. Although the use of NVE simulations guarantees a proper description of velocities of the particles involved in the system, in the general context of this simulation, where the choice of the NVT ensemble was more appropriate, a careful control of the energy exchange with the thermostats employed has permitted a correct evaluation of the VAC functions. Our analysis of the dynamics will be focused on a qualitative manner, just to establish general trends of the spectral properties.

Figure 8 shows the spectra derived from the O and H VAC for simulations A, B, and C. When all the O or H atoms are analyzed, the typical intramolecular and intermolecular bending and stretching modes of the water molecules can be identified. A double peak shaped band in the range of 3000−3500 $cm^{-1}$ may be associated with the symmetric and asymmetric intramolecular O−H stretching modes, whereas a sharp band in the region 1450−1650 $cm^{-1}$ corresponds to the intramolecular HOH bending modes. The band in the region 400−1000 $cm^{-1}$ is characteristic of the intermolecular normal mode contributions of the water network.

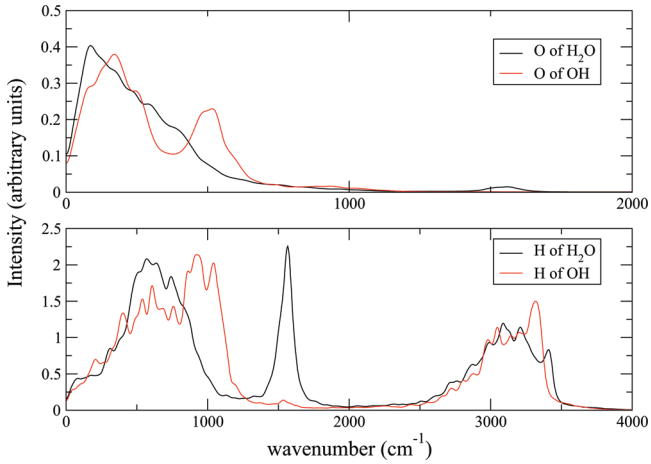


**Figure 9.** Top: Power spectra of the O atoms of the first solvation shell for simulation A. Bottom: Power spectra of the H atoms of the first solvation shell for simulation A.

Our simulation data allow us to extract the dynamical behavior of O and H atoms of the first hydration shell and analyze them separately from the bulk. It is also possible to compare the average spectra derived from atoms of water molecules and hydroxyl groups. On the basis of Figures 3 and 7, we have classified O of the first solvation shell into two categories. The first one is composed by the O atoms that belong to water molecules most of the simulation time, as detailed in the analysis of Figure 7. The rest of the O atoms were considered in the second category, that is, O atoms that belong to hydroxyl groups for most of the simulation time or are involved in the protolysis processes. The comparison of the spectra derived from these two types of oxygen atoms is displayed in Figure 9 (top). For the sake of simplicity, only results from simulation A have been included in this figure. Clear differences between the two spectra appear. Although it is a difficult matter to deal with the identification of dynamical variables associated with the different bands of the spectra, the combined information obtained from FT of the VAC and Po−O first-shell distance autocorrelation functions (not shown in this work) as well as results derived from QM calculations of the frequencies of clusters in the gas phase allow some assignments. In Figure 9 (top), the spectra from the O VAC function of the water molecules presents a wide band between 0−400 $cm^{-1}$ corresponding among other modes to the Po−O stretching, whereas the contribution at a wavenumber of ∼500 $cm^{-1}$ is far less important. A weak band at 1500 $cm^{-1}$ corresponding to the intramolecular HOH bending is present as well. In the case of the O atom of the hydroxyl groups, Po−O stretching appears at 500 $cm^{-1}$. This band at a higher wavenumber than the Po−O($H_2O$) one reflects that the Po−O(OH) bond is stronger in the case of the hydroxyl groups than in the case of the water molecules. Obviously, there is no band at 1500 $cm^{-1}$ in the spectra of the O atom of the hydroxyl groups because of the absence of intramolecular HOH bending.

In the case of the H atoms, the VDOS spectra derived from the first shell of simulation A are included in Figure 9(bottom). For the sake of simplicity, the H atoms involved in the protonation/deprotonation processes have not been included. It is worth mentioning the band at ∼1000 $cm^{-1}$ for the H atoms belonging to hydroxyl groups that is not present in the case of the water molecules and would allow, to certain extent, the identification of $OH^-$ groups around the Po ion. Unfortunately, the direct assignment of these $OH^-$ groups in the first hydration shell of the Po ion can not be easily performed due to the fact that other bands associated with $H_2O$ molecules and $OH^-$ groups and with the ligands going through the protonation and deprotonation processes appear at roughly the same wavenumber. Nonetheless, the subtraction of the solvent contribution based on difference spectra[44,45] could help for the proper characterization of Po-ligand bands in the spectrum of aqueous solutions.

## 4. Concluding Remarks

The present work reports an AIMD study of polonium aqueous solutions, where three different starting hydrolysis degrees of the Po(IV) aquaion were considered. After the time evolution of these systems, a final common arrangement of Po ions in solution is achieved. Our results show that under our medium conditions the coordination number of Po ions in aqueous solution is six. It is also concluded that under our simulation conditions there is not a unique predominant species in solution, but rather an equilibrium among hydroxoaquaions ($[Po(H_2O)_4(OH)_2]^{2+}$ and $[Po(H_2O)_3(OH)_3]^{+}$). Hataye and coworkers[9,10] have experimentally described a rather complex equilibrium involving, among others, these two hydrolyzed forms. Unfortunately, a quantitative comparison with these unique experimental results can not be done because a quantitative pH estimation in our CPMD simulations is not possible. Equilibrium between hydrolyzed forms takes place through a series of protonation and deprotonation processes that involve different ligands in the cluster. The predominant aggregates present a distorted octahedral geometry where hydroxyl ligands avoid being opposite to each other. The Po−O distances of the first solvation shell are not independent to each other so that $OH^-$ ligands exert a trans influence on the water molecule opposite to them causing a lengthening of its Po−O($H_2O$) bonds. This fact is illustrated when a $OH^-$ group is protonated and the Po−O distance of the water molecule in a trans position decreases its value or when a water molecule is deprotonated and the water molecule opposite to it increases its Po−O distance. The structural picture of the simulated solution is in agreement with previous QM results obtained using a semicontinuum solvation model,[15,16] as well as with QM studies on the tetravalent Th(IV) aqua ion, carried out by Tsushima et al.[46,47] Although previous studies[16] show that the coordination number of Po significantly decreases as the stepwise hydrolysis reaction proceeds, the dynamics description supplied by the CPMD simulations allows us to gain insight into this behavior by adding time evolution: the dehydration process occurs after the hydrolysis process has taken place. It is worth pointing out that this is the first time that a sequence of coupled dehydration/deprotonation processes has been reported, as a consequence of dealing with a tetravalent cation in water, that is, we are in a rather extreme case of acidity of the corresponding aquaion.

The characterization of different ligands around the Polonium ion could be done on the basis of difference vibrational spectra mainly due to the bands at 500 and 1000 $cm^{-1}$.

The theoretical description of this very rare tetravalent cation in aqueous solution provided by this study points out to a physicochemical metalloid behavior for polonium in this oxidation state. However, the microscopical description of the aquaion hydrolysis is only the first step to gain insight into the complex solution chemistry of a tetravalent cation such as Po(IV). Further improvements must be envisaged in the direction of including macroscopical factors. Then, estimation of the free energy of the different equilibria and the evaluation of their successive $pK_a$ values, as well as the inclusion of strategies allowing the monitorization of the pH of the system are clearly next steps to be covered. We hope that future experimental and theoretical

research will benefit from this information and gain insight into the main properties of high oxidation states of polonium in condensed phases.

**Acknowledgment.** Junta de Andalucia is acknowledged for financial support (P06-FQM-01484). Barcelona and CESGA supercomputing centers are acknowledged for the computer time, technical expertise, and assistance.

## References and Notes

(1) Ritchens, D. *The Chemistry of Aqua Ions*; Wiley: Chichester, U.K., 1997.
(2) Baes, C. F., Jr.; Mesmer, R. E. *Hydrolysis of Cations*; Wiley: New York, 1976.
(3) Walther, C.; Cho, H.; Marquardt, C. M.; Neck, V.; Seibert, A.; Yun, J.; Fanghänel, T. *Radiochim. Acta* **2007**, *95*, 7.
(4) Neck, V.; Kim, J. I. *Radiochim. Acta* **2001**, *89*, 1.
(5) Farkas, I. Coordination Chemistry of Actinide and Lanthanide Ions. Doktoral Thesis, KTH, Stokholm, 2001.
(6) Farkas, I.; Grenthe, I.; Bányai, I. *J. Phys. Chem. A* **2000**, *104*, 1201.
(7) Yun, J.; Cho, H.; Neck, V.; Altmaier, M.; Seibert, A.; Marquardt, C. M.; Walther, C.; Fanghanel, T. *Radiochim. Acta* **2007**, *95*, 89.
(8) Walther, C.; Fuss, M.; Buchner, S.; Geckeis, H. *J. Radioanal. Nucl. Chem.* **2009**, *282*, 1003.
(9) Hataye, I.; Suganuma, H.; Sakata, M.; Nagame, Y. *J. Inorg. Nucl. Chem.* **1981**, *43*, 2101.
(10) Hataye, I.; Suganuma, H.; Sakata, M. *J. Inorg. Nucl. Chem.* **1981**, *43*, 2575.
(11) Yang, T.; Tsushima, S.; Suzuki, A. *J. Phys. Chem. A* **2001**, *105*, 10439.
(12) Yang, T.; Tsushima, S.; Suzuki, A. *Chem. Phys. Lett.* **2002**, *360*, 534.
(13) Martínez, J. M.; Pappalardo, R. R.; Sánchez Marcos, E. *J. Am. Chem. Soc.* **1999**, *121*, 3175.
(14) Frick, R.; Pribil, A. B.; Hofer, T.; Randolf, B. R.; Bhattacharjee, A.; Rode, B. M. *J. Phys. Chem.* **2009**, *48*, 3993.
(15) Ayala, R.; Martínez, J. M.; Pappalardo, R. R.; Muñoz-Paez, A.; Sánchez Marcos, E. *J. Phys. Chem. B* **2008**, *112*, 5416.
(16) Ayala, R.; Martínez, J. M.; Pappalardo, R. R.; Muñoz-Paez, A.; Sánchez Marcos, E. *J. Phys. Chem. B* **2009**, *113*, 487.
(17) Martínez, J. M.; Pappalardo, R. R.; Sánchez Marcos, E. *J. Phys. Chem. A* **1997**, *101*, 4444.
(18) Zhan, C. G.; Dixon, D. A. *J. Phys. Chem. A* **2004**, *108*, 2020.
(19) Gutowski, K. E.; Dixon, D. A. *J. Phys. Chem. A* **2006**, *110*, 8840.
(20) Coskuner, O.; Jarvis, E.; Allison, T. C. *Angew. Chem., Int. Ed.* **2007**, *46*, 7853.
(21) Sillanpää, A.; Paivarinta, J. T.; Hotokka, M. J.; Rosenholm, J. B.; Laasonen, K. E. *J. Phys. Chem. A* **2001**, *105*, 10111.
(22) Becke, A. D. *Phys. Rev. A* **1988**, *38*, 3098.
(23) Lee, C.; Yang, W.; Parr, R. G. *Phys. Rev. B* **1988**, *37*, 785.
(24) Goedecker, S.; Teter, M.; Hutter, J. *Phys. Rev. B* **1996**, *54*, 1703.
(25) Hartwigsen, C.; Goedecker, S.; Hutter, J. *Phys. Rev. B* **1998**, *58*, 3641.
(26) Krack, M. *Theor. Chem. Acc.* **2005**, *114*, 145.
(27) Sprik, M.; Hutter, J.; Parrinello, M. *J. Chem. Phys.* **1996**, *105*, 1142.
(28) Troullier, N.; Martins, J. L. *Phys. Rev. B* **1991**, *43*, 1993.
(29) Blumberger, J.; Sprik, M. *J. Phys. Chem. B* **2005**, *109*, 6793.
(30) Louie, G.; Froyen, S.; Cohen, M. *Phys. Rev. B* **1982**, *26*, 1738.
(31) Kleynman, L.; Bylander, D. M. *Phys. Rev. Lett.* **1982**, *48*, 1425.
(32) Marx, D.; Hutter, J. *Ab Initio Molecular Dynamics: Basic Theory and Advanced Methods*; Cambridge University Press: Cambridge, U.K., 2009.
(33) Hockney, R. W. *Methods Comput. Phys.* **1970**, *9*, 126.
(34) Car, R.; Parrinello, M. *Phys. Rev. Lett.* **1985**, *55*, 2471.
(35) Nosé, S. *J. Chem. Phys.* **1984**, *81*, 511.
(36) Nosé, S. *Mol. Phys.* **1984**, *52*, 255.
(37) Hoover, W. G. *Phys. Rev. A* **1985**, *31*, 1695.
(38) CPMD, Copyright IBM Corp. 1990−2008, Copyright MPI fur Festkorperforschung Stuttgart 1997−2001.
(39) Bernasconi, L.; Baerends, E. J.; Sprik, M. *J. Phys. Chem. B* **2006**, *110*, 11444.
(40) Lee, M. S.; Salsbury, F. R., Jr.; Brooks, C. L., III. *Proteins* **2004**, *56*, 738.
(41) Khandogin, J.; Brooks III, C. L. *Biophys. J.* **2005**, *89*, 141.
(42) Nordin, J.; Sullivan, D. J.; Phillips, B. L.; Casey, W. J. *Inorg. Chem.* **1998**, *37*, 4760.
(43) Corbacho, E.; Doltsinis, N.; Marx, D.; Pappalardo, R. R.; Sánchez Marcos, E. *Chem. Phys. Chem* **2008**, *126*, 114105.
(44) Bergström, P. A.; Lindgren, J.; Kristiansson, O. *J. Phys. Chem.* **1991**, *95*, 8575.
(45) Bergström, P. A.; Lindgren, J.; Read, M.; Sandström, M. *J. Phys. Chem.* **1991**, *95*, 7650.
(46) Tsushima, S.; Yang, T.; Mochizuki, Y.; Okamoto, Y. *Chem. Phys. Lett.* **2003**, *375*, 204.
(47) Tsushima, S. *J. Phys. Chem. B* **2008**, *112*, 7080.

JP1010956